

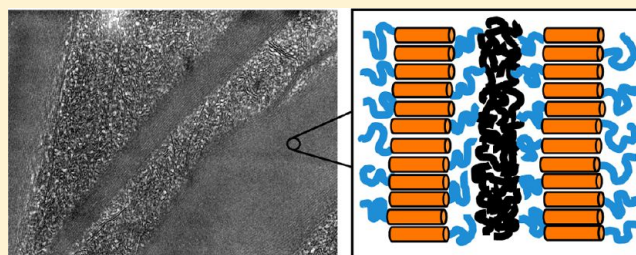
# Phase Behavior of the Blend of Rod–Coil Diblock Copolymer and the Corresponding Coil Homopolymer

Chia-Sheng Lai,<sup>†</sup> Chun-Chih Ho,<sup>‡</sup> Hsin-Lung Chen,<sup>\*,†</sup> and Wei-Fang Su<sup>‡</sup>

<sup>†</sup>Department of Chemical Engineering and Frontier Center on Fundamental and Applied Sciences of Matters, National Tsing Hua University, Hsin-Chu 30013, Taiwan

<sup>‡</sup>Department of Materials Science and Engineering, National Taiwan University, Taipei 10617, Taiwan

**ABSTRACT:** Blending with a homopolymer is an effective approach to tailor the microphase-separated morphology of block copolymers. It has been established for the blends of coil–coil diblock copolymer (A-*b*-B) with the corresponding homopolymer (h-A) that h-A can be solubilized uniformly into A microdomain to induce structure transformation when its molecular weight is smaller than that of the A block, i.e.,  $\alpha = M_{h-A}/M_{b-A} < 1$ . Here we examine if the microdomain structure of a rod–coil diblock copolymer, poly(2,5-diethylhexyloxy-1,4-phenylenevinylene)-*block*-poly(methyl methacrylate) (DEH-PPV-*b*-PMMA), may be systematically tuned by blending with PMMA homopolymer (h-PMMA). The blends over the major composition window were found to undergo macrophase separation even when the value of  $\alpha$  was as low as 0.3. The phase separation led to the formation of a copolymer-rich phase and a homopolymer-rich phase, in which microphase separation occurred, yielding a well-ordered lamellar structure and a sponge structure, respectively. The phase behavior of the blend of rod–coil diblock with the corresponding coil homopolymer is hence fundamentally different from that of the conventional blend of coil–coil diblock in that microdomain morphology transformation induced by completely uniform solubilization of coil homopolymer into the selective microdomain is essentially inaccessible. This fact is attributed to the large positive free energy of mixing between the whole rod–coil diblock and the coil homopolymer due to strong rod–rod attraction, the intrinsically strong repulsion between DEH-PPV and PMMA, and the low entropy of mixing.



## INTRODUCTION

Self-assembly of block copolymers is an effective way to create well-defined nanostructures.<sup>1–3</sup> It is known that the microphase separation in the diblock copolymers composing of two flexible coils (called the “coil–coil diblock copolymer”) can generate a series of long-range ordered microdomains. The morphology formed is dictated by the strength of mutual repulsion between the dissimilar blocks and the packing constraint imposed by the connectivity of each block.<sup>1–3</sup> These effects can be parametrized into two main factors, namely, volume fraction, and segregation strength  $\chi N$ .

Since the domain structure is closely governed by the volume fraction, the microphase-separated morphology of coil–coil diblock copolymer (A-*b*-B) may also be tailored by blending with the corresponding homopolymer (h-A).<sup>4,5</sup> It has been shown that the phase behavior of such a blend is dictated by the molecular weight of h-A ( $M_{h-A}$ ) relative to that of A block ( $M_{b-A}$ ), which is expressed by the factor  $\alpha = M_{h-A}/M_{b-A}$ . The magnitude of  $\alpha$  determines the degree of mixing between A block and h-A.<sup>6</sup> h-A chains dissolve and distribute uniformly in A microdomain to swell the distance between the junction points at the domain interface when  $\alpha < 1$ . This case is known as the “wet brush”. The transformation of B microdomain from lamellae to cylinder to sphere can occur with increasing h-A composition in the wet-brush regime.

When  $M_{h-A}$  is approximately the same as  $M_{b-A}$ , i.e.,  $\alpha \approx 1$ , the “dry-brush” phase behavior is obtained. In this case, h-A chains still enter into A microdomains, but they are localized to the middle regions of the domains, leaving the junction point separation unchanged. In the dry-brush blend of lamellae-forming A-*b*-B and h-A, the thickness of A domain is swollen continuously with increasing h-A composition while retaining the lamellar identity and thickness of B domain. Macrophase separation takes place over a broad range of composition when  $M_{h-A}$  is larger than  $M_{b-A}$ , i.e.,  $\alpha > 1$ .<sup>7,8</sup>

The present study is centered on the phase behavior of the blend of rod–coil diblock copolymer composed of a rigid rod and a flexible coil. The self-organization behavior of rod–coil diblock is different from that of the coil–coil system because of the additional complications arising from the rod–rod interaction and the negligible conformational entropy of the rod block. In this case, the microphase-separated morphology is governed not only by the energy of interaction ( $\chi$ ) between the rod and the coil block but also by the anisotropic interaction of the rods (i.e., the Maier–Saupe interaction) and the geometric mismatch between the coil and the rod which determines the

Received: September 27, 2012

Revised: January 3, 2013

Published: March 7, 2013

degree of stretching of the coil block.<sup>9–13</sup> Theoretical calculations of the phase diagram considering these free energy contributions have predicted that the microphase-separated structure of rod–coil diblock copolymers also depends on the volume fraction of the coil (or rod) block.<sup>14–19</sup> Lamellar morphology was found to form over the major composition window. Hexagonally packed columnar (cylinder) and BCC-packed sphere morphology with the rod block forming the discrete microdomains may develop at high coil volume fraction.<sup>15</sup>

The phase diagrams of high molecular weight rod–coil diblock copolymers have also been studied experimentally using poly(2,5-di(2'-ethylhexyloxy)-1,4-phenylenevinylene) (DEH-PPV) as the rod component. Consistent with the theoretical predictions, the microphase-separated morphology was found to depend on composition. Olsen and Segalman<sup>9–11</sup> have systematically investigated DEH-PPV-*block*-polyisoprene (DEH-PPV-*b*-PI) system which exhibited relatively weak segregation strength. Only lamellar phases were observed as the microphase-separated structure for the low molecular weight sample. For the higher molecular weight materials (which increased the segregated strength), a hexagonal phase of rod aggregates with a rectangular cross section was observed; this hexagonal phase was formed at both high coil fractions and large relative block size characterized by the ratio of the radius of gyration of the coil block to the characteristic rod length. Moreover, the order–disorder transition from the microphase-separated state to the isotropic phase was found to be intervened by a nematic phase. In the cases of strongly segregated rod–coil diblocks, such as DEH-PPV-*block*-poly(4-vinylpyridine) (DEH-PPV-*b*-P4VP)<sup>12</sup> and DEH-PPV-*block*-poly(methyl methacrylate) (DEH-PPV-*b*-PMMA),<sup>13</sup> lamellar morphology was found to span from the rod-rich to the coil-rich regime. Hexagonal and even BCC structures were identified at sufficiently high coil volume fraction ( $f_{\text{coil}} > 0.65$ ).

Since both experimental and theoretical studies have demonstrated that the microphase-separated morphology of rod–coil diblock copolymers depends on composition, it is of interest to inspect if the microdomain structure of the rod block may be systematically tuned by blending with the corresponding coil homopolymer. There were a few studies on the phase behavior rod–coil diblock copolymer/homopolymer blends. Lee and co-workers investigated the blends of oligomeric rod–coil block copolymer composing of poly(ethylene oxide) (PEO) coil block and PEO homopolymer (h-PEO).<sup>20</sup> They found that h-PEO was able to solubilize into PEO microdomains, as manifested by the swelling of domain spacing upon the addition of h-PEO. Nevertheless, the increase of domain spacing saturated at high homopolymer volume fraction, suggesting the existence of a solubility limit which decreased with increasing molecular weight of h-PEO. Tao et al.<sup>21</sup> studied the blends of a weakly segregated lamellae-forming DEH-PPV-*b*-PI with the corresponding coil and rod homopolymers bearing the same molecular weights as those of the corresponding blocks in the copolymer (i.e.,  $\alpha \approx 1$ ). They found that while adding coil homopolymer to the copolymer increased the domain spacing by swelling the coil domain, adding rod homopolymer decreased the domain spacing due to interdigitation of rods within the lamellar microdomain. The authors also demonstrated that these experimental observations were consistent with the prediction of the self-consistent field theory. Sary et al.<sup>22</sup> studied the blend of DEH-PPV homopolymer with DEH-PPV-*b*-PS. Long-range ordered

microphase-separated structure was observed until over 40% of DEH-PPV was added to cause a macrophase separation. They also investigated the blends of poly(3-hexylthiophene)-*block*-poly(4-vinylpyridine) (P3HT-*b*-P4VP) rod–coil diblock copolymer with a C<sub>60</sub> material, [6,6]-phenyl-C61-butyric acid methyl ester (PCBM), in which C<sub>60</sub> molecules were selectively solubilized into the P4VP domains due to their favorable interactions.<sup>23</sup> The blends were found to exhibit a kind of bicontinuous sponge structure without showing macrophase separation.

We found that the previous studies of the blends of rod–coil block copolymers with coil or rod homopolymers usually dealt with the homopolymers with similar molecular weights to the corresponding blocks in the copolymers. In this case, the swelling of domain spacing was the major concern for assessing the solubilization of homopolymer into the corresponding microdomain. A critical issue regarding the phase behavior of the rod–coil block copolymer/homopolymer blend in terms of the effect of the magnitude of  $\alpha$  remains unresolved. We are hence interested in the problem as to whether the blend of rod–coil diblock copolymer with the corresponding coil homopolymer would behave similarly to the coil–coil blend where a transformation of microdomain morphology may be accessed when the molecular weight of the coil homopolymer is sufficiently low (to reach the wet-brush regime). Therefore, here we undertake a systematic study of the phase behavior of a strongly segregated lamellae-forming DEH-PPV-*b*-PMMA with PMMA homopolymers (h-PMMA) with various molecular weights. The values of  $\alpha$  investigated here ranged from 0.31 to 1.25. It will be shown that, in contrast to the conventional coil–coil blends, the blend system under study exhibited macrophase separation over the major composition window irrespective of the value of  $\alpha$ . The macrophase separation yielded a copolymer-rich phase and a homopolymer-rich phase, in which microphase transition generating a well-ordered lamellar structure and a sponge nanostructure, respectively, occurred. The order–disorder transitions of the nanostructures formed were also investigated.

## ■ EXPERIMENTAL SECTION

The synthesis of DEH-PPV-*b*-PMMA used in the present study has been described elsewhere.<sup>13</sup> The volume fraction of PMMA block in the diblock was 0.3. PMMA homopolymers were acquired from Polymer Laboratories Inc. or Polymer Source Inc. Table 1 summarizes the characteristics of h-PMMA and diblock copolymer samples used.

**Table 1. Molecular Characteristics of the DEH-PPV-*b*-PMMA and PMMA Homopolymers Used in the Present Study**

sample	DEH-PPV $M_n$ (g/mol)	PMMA $M_n$ (g/mol)	$f_{\text{PMMA}}$	$M_w/M_n$
DEH-PPV- <i>b</i> -PMMA	3850	2030	0.3	1.1
h-PMMA1		625	1.0	1.3
h-PMMA2		1100	1.0	1.2
h-PMMA3		2500	1.0	1.1

The blends of DEH-PPV-*b*-PMMA with h-PMMA were prepared by first dissolving a predetermined amount of the copolymer and h-PMMA in dichloromethane followed by slowly evaporating the solvent at room temperature. The composition of the blend was denoted by  $f_b$ , which signified the overall volume fraction of the diblock in the blend (the volume fraction of h-PMMA was hence  $1 - f_b$ ). The blends with

$f_b$  ranging from 0.29 to 0.86 were prepared. The dried blend samples were further annealed under nitrogen atmosphere at 175 °C for 24 h.

SAXS measurements were performed using a Bruker Nanostar SAXS instrument. The X-ray source, a 1.5 kW X-ray generator (Kristalloflex 760) equipped with a Cu tube, was operated at 35 mA and 40 kV. The scattering intensity was detected by a two-dimensional position-sensitive detector (Bruker AXS) with  $512 \times 512$  channels. The area scattering pattern has been radially averaged to increase the photon counting efficiency compared with the one-dimensional linear detector. The intensity profile was output as the plot of the scattering intensity ( $I$ ) vs the scattering vector,  $q = 4\pi/\lambda \sin(\theta/2)$  ( $\theta$  = scattering angle). All scattering data were corrected by the empty beam scattering, the sensitivity of each pixel of the area detector, and thermal diffuse scattering.

Temperature-dependent SAXS experiments for probing the order–disorder transitions in the blends were performed at Beamline 23A1 at the National Synchrotron Radiation Research Center (NSRRC) located at Hsin-Chu, Taiwan. A two-dimensional Mar CCD detector with  $512 \times 512$  pixel resolution was used to record the SAXS pattern. The energy of the X-ray source ( $\lambda = 0.124$  nm) and the sample-to-detector distance were 10 keV and 1886 mm, respectively. The beam center was calibrated using silver behenate with the primary reflection peak at  $1.067$  nm $^{-1}$ . Temperature-dependent SAXS/WAXS measurements were performed under a nitrogen-purged atmosphere with the accuracy of temperature control of  $\pm 0.5$  °C.

The real-space morphology of the blends was examined by a JEOL JEM-1230 TEM operated at 100 kV. The blending specimens were first embedded in epoxy resin and were then microtomed at room temperature with a Reichert Ultracut E sectioning system. The microtomed sections were collected onto copper grids coated with Formvar and carbon-supporting films followed by staining with RuO $_4$  vapor for 5 min. Since RuO $_4$  was a preferential staining agent for DEH-PPV block, DEH-PPV and PMMA domains appeared as dark and bright regions in the micrographs, respectively.

Large-amplitude oscillatory shear (LAOS) was performed to produce large-scale alignment of the microdomains in neat DEH-PPV-*b*-PMMA. The shearing was carried out being a Linkam CSS 450 shear hot stage in the oscillatory mode with the shear frequency of 0.5 Hz and the strain amplitude of 80%.

## RESULTS

**Self-Organization Behavior of Neat DEH-PPV-*b*-PMMA.** Before presenting the phase behavior of DEH-PPV-*b*-PMMA/h-PMMA blends, it is useful to consider the self-organization behavior of the neat DEH-PPV-*b*-PMMA to verify the rodlike conformation of DEH-PPV blocks in the lamellar microdomains. Figure 1 displays the SAXS and WAXS profiles of the rod–coil diblock used in the present study. The SAXS profile shows a pair of diffraction peaks with the position ratio of 1:2, indicating the formation of a lamellar morphology. The thicknesses of DEH-PPV and PMMA lamellae were 5.54 and 3.38 nm, respectively, as obtained by fitting the SAXS intensity data using a paracrystalline model developed by Förster et al.,<sup>24</sup> which takes into account the domain size distribution, distortion of domain spacing, grain size, and peak shape which varied analytically between Lorentzian and Gaussian functions. The WAXS pattern of the diblock shows the characteristic diffraction peaks associated with the tetragonal unit cell of the crystalline phase of DEH-PPV.<sup>25</sup>

Since DEH-PPV block is crystalline in the lamellar microdomain, it is important to understand the orientation of the crystalline stems with respect to the lamellar interface, as such an orientation would determine the cross-sectional area of the junction points and hence the degree of stretching of PMMA block (which may in turn affect the extent of solubilization of h-PMMA due to the interplay between the conformational entropy and the entropy of mixing). To reveal

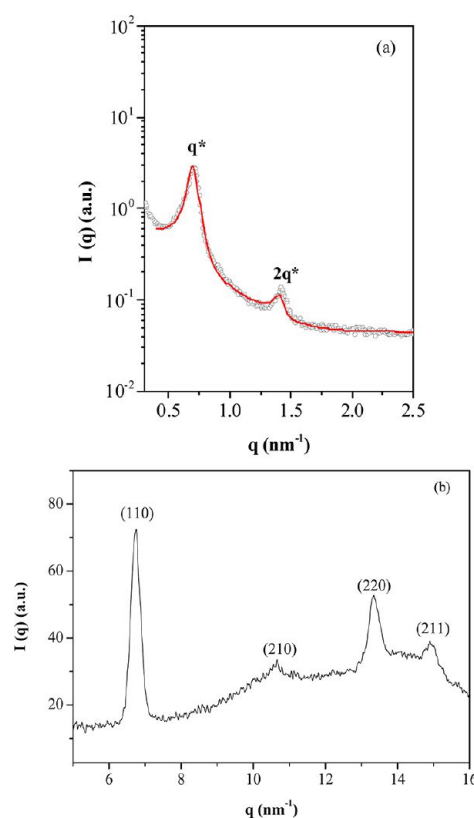


**Figure 1.** (a) SAXS and (b) WAXS profiles of neat DEH-PPV-*b*-PMMA ( $f_{\text{PMMA}} = 0.3$ ) collected at room temperature. The solid curve superposing on the experimental SAXS data represents the fit by the paracrystalline model of lamellar structure.

the stem orientation, the copolymer was first subjected to the large-amplitude oscillatory shear (LAOS) at 180 °C for 2 h to produce a large-scale alignment of the lamellar microdomains in the sample. 2-D SAXS and WAXD patterns of the sheared sample were then obtained to identify the orientation of DEH-PPV stems with respect to the lamellar interface.

Figure 2a shows the representative 2-D SAXS pattern of the sample collected at 30 °C. The pattern shows a pair of reflections at the equator, indicating that the lamellar domains in the sheared sample were macroscopically aligned. The SAXS pattern remained unchanged upon heating as long as the temperature situated below the order–disorder transition temperature of the microphases.

Figure 2b displays the corresponding 2-D WAXD pattern of the DEH-PPV-*b*-PMMA. The (110) reflection was found to locate preferentially in the meridian. The azimuthal scans of the intensities of the primary reflection in the SAXS pattern and the (110) diffraction in the WAXD pattern shown in Figure 2c reveal more clearly the orientation of the (110) plane with respect to the lamellar interface. It can be seen that the primary peak intensity of the SAXS pattern located predominantly at the azimuthal angle of 0° and 180°, while the intensity of (110) peak in the WAXD pattern situated preferentially at –90° and 90°. The fact that the intensity distributions of these two scattering peaks were orthogonal to each other signaled that the DEH-PPV stems oriented perpendicularly to the lamellar interface.<sup>26</sup>

Since the DEH-PPV stems oriented normal to the lamellar interface and the thickness of the lamellar domain (5.54 nm) was comparable to the contour length of the block chain (~6

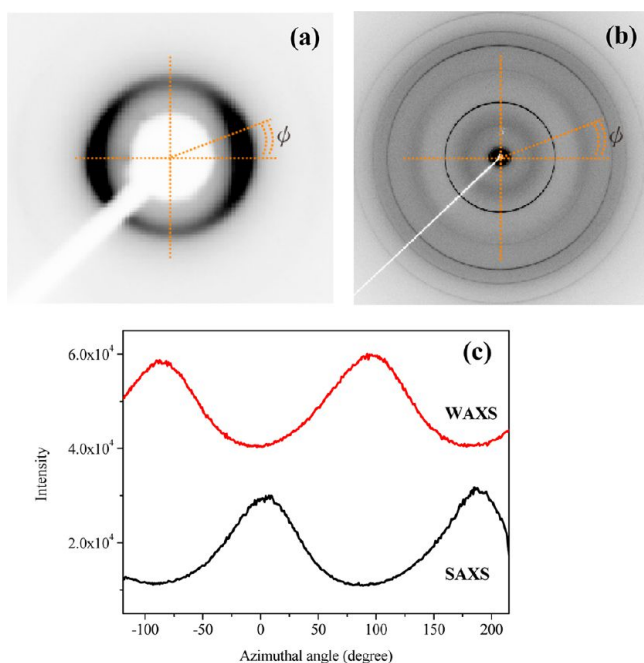


**Figure 2.** The representative 2-D (a) SAXS and (b) WAXS pattern of neat DEH-PPV-*b*-PMMA after subjecting to large-amplitude oscillatory shear treatment. (c) The corresponding azimuthal scans of the intensities of the SAXS primary peak and WAXS (110) reflection. The azimuthal angle  $\phi$  is defined on the 2-D scattering patterns.

nm), the DEH-PPV blocks in the lamellar microdomains should adopt rodlike conformation and the microdomains composed of a monolayer of DEH-PPV rods.

Intuitively, the rodlike conformation of DEH-PPV should prescribe a small cross-sectional area of the junction point, so as to cause a large stretching of PMMA blocks. Knowing the monolayer arrangement of DEH-PPV block in the lamellar microdomain, we calculated the reduced tethering density of PMMA blocks to examine if they were highly stretched. The reduced tethering density is defined as the ratio of the cross-sectional area of the unperturbed PMMA chain to that of the junction points at the lamellar interface ( $\Sigma$ ),<sup>27</sup> i.e.

$$\sigma = \pi R_g^2 / \Sigma \quad (1)$$

where  $R_g$  is the unperturbed radius of gyration of PMMA.<sup>28</sup>  $\Sigma$  is given by

$$\Sigma = \frac{m_{\text{PMMA}}}{d_{\text{PMMA}} \rho_{\text{PMMA}}} \quad (2)$$

where  $d_{\text{PMMA}}$ ,  $\rho_{\text{PMMA}}$ , and  $m_{\text{PMMA}}$  are the thickness of PMMA microdomain, the melt density of PMMA, and the mass of a PMMA block, respectively. The value of  $\sigma$  calculated by eq 1 was 5.04. This value was larger than 1, signaling that PMMA blocks did stretch normal to the lamellar interface; however, the fact that it was obviously smaller than the critical value of the onset of highly stretched brush regime ( $>14.3$ )<sup>27</sup> indicates that the PMMA blocks were not strongly stretched. Hence, the cross-sectional area of the junction points was not as small as that expected intuitively since the side chains of DEH-PPV increased the lateral dimension of the rods.

#### Miscibility between DEH-PPV-*b*-PMMA and h-PMMA.

Here we investigate the miscibility between DEH-PPV-*b*-PMMA and h-PMMA with various molecular weights to reveal if the transformation of the microdomain structure of DEH-

PPV block may be accessed under certain conditions. The value of  $\alpha$  covered here ranged from 0.31 to 1.23.

We first examine the miscibility of the blends with the h-PMMA3 having the molecular weight of 2500 g/mol ( $\alpha = 1.23$ ). Figure 3a displays the SAXS profiles of this blend system

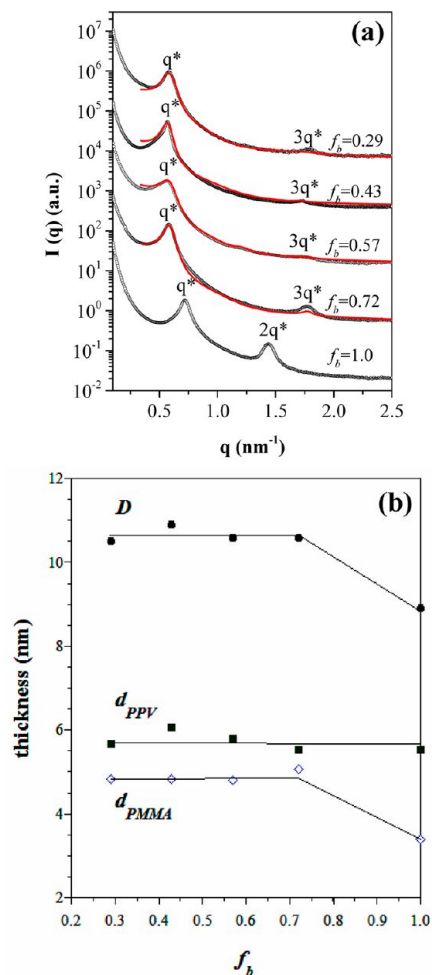


**Figure 3.** (a) SAXS profiles of DEH-PPV-*b*-PMMA/h-PMMA1 blends ( $\alpha = 1.23$ ). (b) Composition variations of the interlamellar distance ( $D$ ) and the thickness of DEH-PPV ( $d_{\text{PPV}}$ ) and PMMA ( $d_{\text{PMMA}}$ ) microdomain of the well-ordered lamellar structure formed in the copolymer-rich phase. The solid curves superposing on the experimental SAXS data represent the fit by the paracrystalline model of lamellar structure.

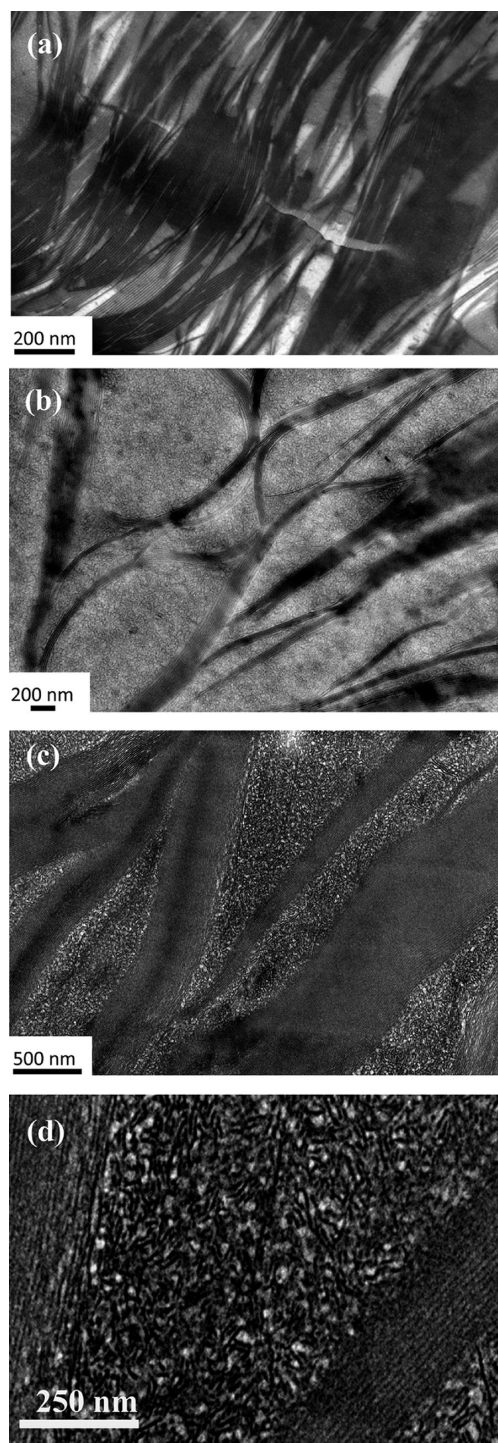
with the composition expressed by the overall volume fraction of the diblock ( $f_b$ ). Over the composition range investigated, the SAXS profiles displayed a pair of diffraction peaks with the position ratio of 1:3, signaling that the blends still exhibited lamellar morphology with approximately equal volume fraction of the rod and coil domain. The primary scattering peak of the lamellar structure was found to shift from  $0.7 \text{ nm}^{-1}$  (for neat diblock) to  $0.58 \text{ nm}^{-1}$  upon the addition of a small amount of h-PMMA ( $f_{\text{h-PMMA}} = 0.28$ ), indicating a swelling of the interlamellar distance ( $D$ ) from 9 to 10.8 nm due to solubilization of h-PMMA into PMMA microdomain. The solubilization of h-PMMA appeared to saturate at a certain extent, as the position of the primary peak remained unchanged upon further increase of h-PMMA content.

Figure 3b plots  $D$ , the thickness of DEH-PPV layer ( $d_{\text{PPV}}$ ), and the thickness of PMMA layer ( $d_{\text{PMMA}}$ ) obtained from the model fitting as a function of  $f_b$ . It can be seen that  $d_{\text{PMMA}}$  increased upon blending with h-PMMA, but its value leveled off at ca. 4.8 nm, confirming that there was a limit in the extent of solubilization of PMMA homopolymer in the coil lamellar microdomain.  $d_{\text{PPV}}$  was found to be largely unperturbed by blending with h-PMMA. For the coil-coil diblock blends, this is a signature of the dry-brush type of mixing between the coil block and the corresponding homopolymer;<sup>6</sup> therefore, h-PMMA chains in the coil microdomains should be localized to the middle region in the domain due to higher molecular weight than that of PMMA block.

The fact that there existed a limited extent of solubilization of h-PMMA indicated that the blends should exhibit a macrophase separation over the composition range studied, leading to a diblock copolymer-rich phase and an h-PMMA-rich phase. The occurrence of macrophase separation was confirmed by the representative TEM micrograph in Figure 4a. Here the copolymer-rich phase corresponded to the macrodomains composing of well-ordered lamellar microdomains (which gave rise to the multiple diffraction peaks in the SAXS profiles), and the brighter regions were the h-PMMA-rich phase. It is noted that the lamellar microdomains exhibited relatively large persistence length and thereby gave rise to macrodomains with fibrillar shape.

Now we consider the blends with h-PMMA2 having the molecular weight of 1100 ( $\alpha = 0.54$ ). Figure 5a displays the SAXS profiles of the blends as a function of composition. In contrast to the system with  $M_{\text{h-PMMA}} = 2500$ , two characteristic sets of scattering patterns were observed. One of them is characterized by two diffraction peaks with the position ratio of 1:3, signaling the existence of a well-ordered lamellar morphology in the blends. An additional peak (pinpointed by the arrows in Figure 5a) was identified at ca.  $0.25\text{--}0.3\text{ nm}^{-1}$ , showing that an additional nanostructure with the characteristic interdomains distance of ca. 25 nm developed in the blends. The values of  $D$ ,  $d_{\text{PPV}}$ , and  $d_{\text{PMMA}}$  associated with the well-ordered lamellar structure obtained from model fitting were plotted as a function of  $f_b$  in Figure 5b. In this case, the scattering profiles starting from  $q$  slightly smaller than the primary peak position ( $q^*$ ) were used for the fitting. Although the overlap with the additional low- $q$  peak may perturb the shape of the primary peak of the well-ordered lamellar structure, the thickness of the domains in the lamellar stack obtained from the fitting is still reliable since its value (which is smaller than the interlamellar distance) is governed by the profile at the higher  $q$  region ( $q > q^*$ ) which is much less affected by the additional low- $q$  peak. Because the value of  $D$  is determined by  $q^*$ , which should not be perturbed significantly by the overlap with the low- $q$  peak, the values of  $D$ ,  $d_{\text{PPV}}$ , and  $d_{\text{PMMA}} (= D - d_{\text{PPV}})$  obtained for the well-ordered lamellar structure were reliable.

As can be seen in Figure 5b, the PMMA domain thickness was found to increase upon the addition of h-PMMA, but it leveled off at  $f_b \sim 0.57$ . This fact revealed that h-PMMA was incorporated into the PMMA lamellar microdomains, but there was again a limit in the extent of solubilization. However, the degree solubilization saturated at a higher homopolymer composition ( $f_{\text{h-PMMA}} \sim 0.43$ ) compared to the blend with h-PMMA3. The thickness of DEH-PPV domain was basically unperturbed by the blending, implying that h-PMMA and



**Figure 4.** Representative TEM micrographs of the blends of DEH-PPV-*b*-PMMA with (a) h-PMMA3 ( $f_b = 0.72$ ), (b) h-PMMA2 ( $f_b = 0.57$ ), and (c) h-PMMA1 ( $f_b = 0.43$ ). The micrograph in (d) shows the enlarged image of the sponge structure formed in h-PMMA 1 blend with  $f_b = 0.43$ .

PMMA blocks formed dry-brush mixture in the PMMA lamellar microdomains.<sup>6</sup>

The formation of two types of nanostructure revealed by SAXS indicated the presence of two types of macrophases; in other words, the blends still exhibited macrophase separation although the value of  $\alpha$  was obviously smaller than 1.0. Figure 4b shows the representative TEM micrograph of the blend with

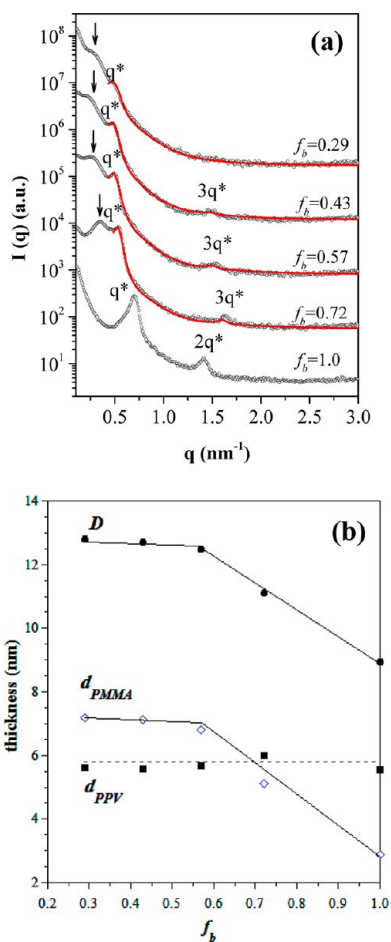


**Figure 5.** (a) SAXS profiles of DEH-PPV-*b*-PMMA/h-PMMA2 blends ( $\alpha = 0.54$ ). (b) Composition variations of the interlamellar distance ( $D$ ) and the thickness of DEH-PPV ( $d_{PPV}$ ) and PMMA ( $d_{PMMA}$ ) microdomain of the well-ordered lamellar structure formed in the copolymer-rich phase.

$f_b = 0.57$ . It is clear that the blend underwent a macrophase separation, generating again a copolymer-rich phase in which a microphase transition took place to yield well-ordered lamellar microdomains (similar to the blend with  $\alpha = 1.23$ ). The other macrophase generated by the phase separation was the h-PMMA-rich phase. In contrast to the blend with  $\alpha = 1.23$  (where no clear internal nanostructure was identified from the TEM micrograph), a “sponge nanostructure” with interconnecting DEH-PPV domain was observed in this macrophase. A close examination of the dark DEH-PPV microdomains forming the sponge structure revealed that these domains were highly distorted lamellae (as can be seen more clearly in Figure 4d for the blend with h-PMMA1). The sponge structures formed in surfactants and coil–coil diblock copolymer systems have been characterized in previous studies.<sup>29,30</sup> In contrast to the gyroid structure, the basic entity constructing the network in the sponge phase is more or less layer in geometry. In the blend system under study, the DEH-PPV domains in the h-PMMA-rich phase showed lamellar entity and were extensively interconnected; therefore, the term “sponge phase” is appropriate for describing the structure formed in this macrophase. The characteristic interdomain distance of ca. 25 nm in the sponge structure gave rise to the low- $q$  peak at ca.  $0.25 \text{ nm}^{-1}$ . Since the DEH-PPV domain retained its lamellar entity, the PMMA blocks surrounding

these distorted lamellae should interact with the h-PMMA chains through dry brush.

Our results for the blends with  $\alpha = 0.54$  revealed that the blends of the rod–coil diblock copolymer with the corresponding homopolymer show different phase behavior from that of the corresponding coil–coil diblock copolymer blends. Although the molecular weight of h-PMMA was significantly lower than that of PMMA block ( $\alpha = 0.54$ ), the blends still exhibited a macrophase separation over the major composition window.

To examine if complete solubilization of h-PMMA may eventually be accessed to induce the morphological transition of DEH-PPV microdomain, we further investigated the blend with h-PMMA1 where the  $\alpha$  value was as low as 0.31. Figure 6a

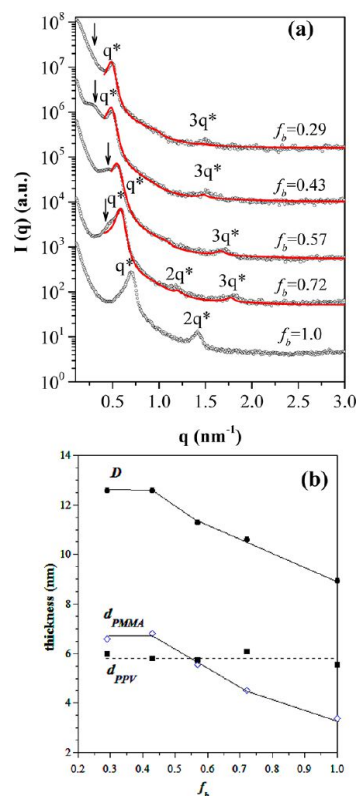


**Figure 6.** (a) SAXS profiles of DEH-PPV-*b*-PMMA/h-PMMA1 blends ( $\alpha = 0.31$ ). (b) Composition variations of the interlamellar distance ( $D$ ) and the thickness of DEH-PPV ( $d_{PPV}$ ) and PMMA ( $d_{PMMA}$ ) microdomain of the well-ordered lamellar structure formed in the copolymer-rich phase.

shows the SAXS profiles of this blend system. It can be seen that the SAXS patterns exhibited essentially the same features as those for the blend with  $\alpha = 0.54$ , where two sets of scattering peaks corresponding to a well-ordered lamellar structure and a sponge structure were observed. The existence of these two types of nanostructures was again verified by the TEM micrograph in Figure 4c,d. The composition dependences of the interlamellar distance and domain thicknesses associated with the well-ordered lamellar structure shown in Figure 6b revealed that there was again a limit in the extent of solubilization of h-PMMA into the PMMA lamellar domains, but the saturation point moved further to even lower  $f_b$  ( $f_b = 0.43$ ).

The systematic examination of the effect of  $\alpha$  on the degree of solubilization of h-PMMA has disclosed that the blends of DEH-PPV-*b*-PMMA with h-PMMA underwent macrophase separation over the major composition window even for small  $\alpha$ . Figure 7 summarizes the observed interlamellar distances of

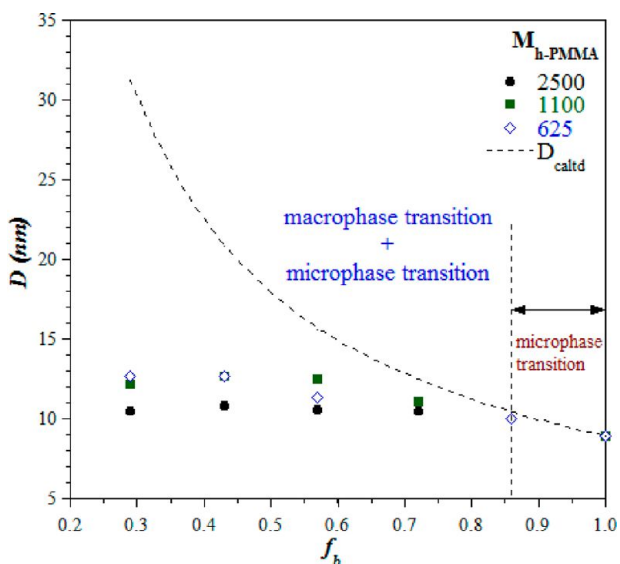


**Figure 7.** Comparison between the observed interlamellar distances of the well-ordered lamellar structure and the calculated values for complete solubilization of h-PMMA (---). The difference becomes clear at  $f_b < 0.86$ .

the well-ordered lamellar structure as a function of  $f_b$ . The interlamellar distance expected for complete solubilization of h-PMMA into the lamellar domains calculated by  $D_{\text{calcd}} = d_{\text{PPV}}/f_{\text{PPV}}$  (with  $f_{\text{PPV}}$  being the overall volume fraction of DEH-PPV) was also plotted for comparison. When  $f_b$  was higher than 0.86, the observed  $D$  agreed well with the predicted value for complete solubilization; in this case, the blend was a single-phase system showing only microphase transition. The observed  $D$  started to deviate from  $D_{\text{calcd}}$  at  $f_b \sim 0.72$ , indicating that DEH-PPV-*b*-PMMA became immiscible with h-PMMA, and the blends exhibited macrophase separation.

**Thermally Induced Phase Transition of DEH-PPV-*b*-PMMA/h-PMMA Blends.** Temperature-dependent simultaneous SAXS/WAXS experiments were conducted to examine if the blends exhibit any thermally induced phase transition. Figures 8a and 8b show the representative temperature-dependent SAXS and WAXS profiles for the blend with  $\alpha = 0.54$  and  $f_b = 0.72$  collected in a heating and subsequent cooling cycle, respectively. In the heating cycle, the intensities of the primary peaks associated with the sponge structure and the well-ordered lamellar structure were found to decrease with increasing temperature; meanwhile, the intensity of (110) peak in the WAXS profile (see Figure 8b) also showed similar trend. At 200 °C, only a broad peak was observed in the SAXS profile, indicating that the microphases in the respective macrophase became disordered. The (110) crystalline peak also vanished at this temperature due to melting of DEH-PPV crystallites. The temperature-dependent SAXS results thus revealed an order-disorder transition (ODT) of the microphases formed in the two types of macrophases. The ODT appeared to coincide the melting of the crystallites.

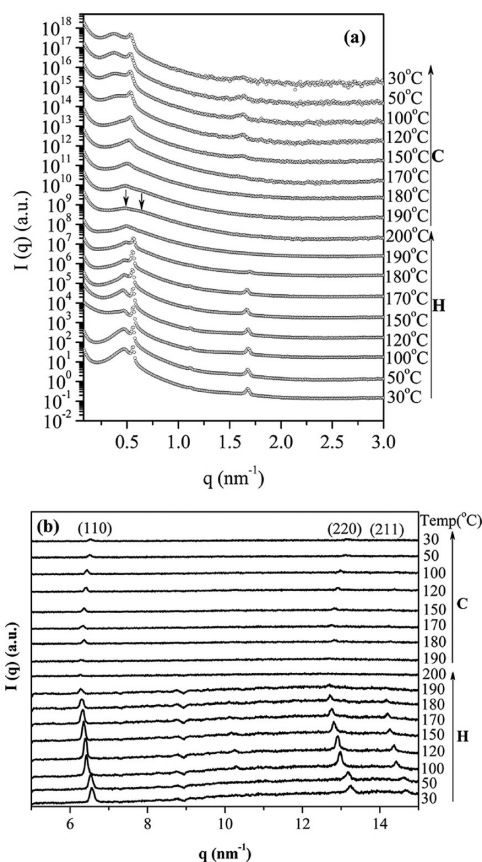


**Figure 8.** Temperature-dependent (a) SAXS and (b) WAXS profiles of DEH-PPV-*b*-PMMA/h-PMMA2 blend ( $f_b = 0.72$ ) collected simultaneously in a heating (denoted by “H” in the figure) and cooling (denoted by “C” in the figure) cycle.

Figure 9 plots the inverse of the intensities of the two primary SAXS peaks and (110) peak in the WAXS profiles against the inverse of absolute temperature for determining the

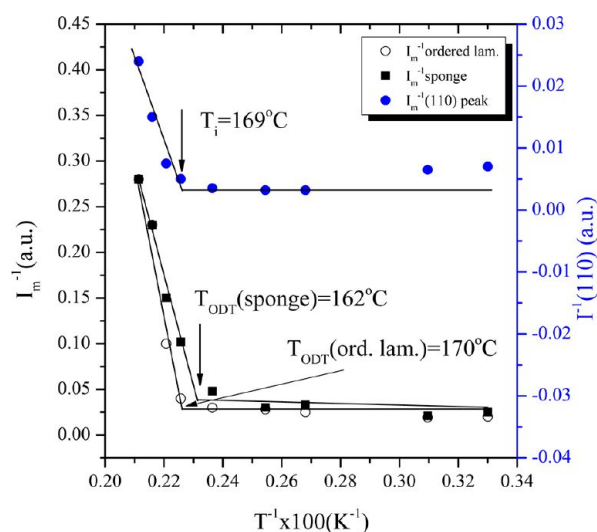


**Figure 9.**  $I_m^{-1}$  vs  $T^{-1}$  plots using the SAXS and WAXS data collected in the heating cycle for the determinations of the  $T_{\text{ODT}}$  of the well-ordered lamellar structure and sponge structure and the melting point of DEH-PPV crystallites for DEH-PPV-*b*-PMMA/h-PMMA2 blend ( $f_b = 0.72$ ).

order–disorder transition temperatures ( $T_{\text{ODT}}$ ) of the well-ordered lamellar structure and the sponge structure as well as the crystal melting point. The  $T_{\text{ODT}}$ s of the sponge phase and well-ordered lamellar phase were found to situate at 162 and 170 °C, respectively, and the melting point determined from the intensity of (110) peak located at ca. 169 °C.

Upon the disordering of the two microphases, the two disordered phases may mix together to form a single homogeneous disordered phase or the blends may still be phase-separated and composed of two disordered macrophases with different compositions. A close examination of the broad SAXS peak observed at 200 °C revealed that the peak actually contained two correlation hole peaks (marked by the arrows in Figure 8a) associated with the characteristic concentration fluctuations in the respective two macrophases. Therefore, the blends were macrophase-separated even after disordering the microphase-separated structure.

Figure 8 also shows the SAXS and WAXS profiles collected in the subsequent cooling cycle (i.e., the sample was cooled from the disordered state at 200 °C). It can be seen that the two sets of SAXS peaks associated with the sponge structure and well-ordered lamellar structure recovered upon the cooling. However, the crystallinity DEH-PPV developed during the cooling was much lower than that at the beginning of the heating experiment. This fact indicates that the microphase separations occurred in the two types of macrophases were not driven mainly by the crystallization of DEH-PPV, but rather by the intrinsic repulsion (prescribed by the large  $\chi$  value) between DEH-PPV and PMMA.

## DISCUSSION

Figure 10 schematically illustrates the phase diagram of the DEH-PPV-*b*-PMMA/h-PMMA blends. The diagram was

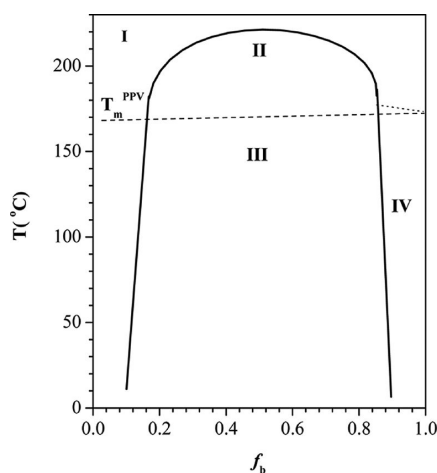


**Figure 10.** Proposed phase diagram of the DEH-PPV-*b*-PMMA/h-PMMA blends. Region I: homogeneous disordered phase (one phase). Region II: biphasic state without microphase separation. Region III: biphasic state with microphase separation in the macrophases. Region IV: single-phase state with microphase separation.

adopted from that of the conventional blend of the coil–coil diblock copolymer with a homopolymer.<sup>7</sup> The four regions shown in the phase diagram are the following: region I: homogeneous disordered phase (one phase); region II: biphasic state without microphase separation; region III:

biphasic state with microphase separation in the macrophases; region IV: single-phase state with only microphase separation.

The phase diagram shows that the blends display macrophase separation over the major composition and temperature window. The macrophase separation yielded a homopolymer-rich phase and a copolymer-rich phase. Driven by the strong repulsion between DEH-PPV and PMMA, microphase transition occurred within the macrophases, generating a well-ordered lamellar nanostructure and a sponge phase in the respective macrophases. Therefore, a coupling between macrophase separation and microphase transition is operative within the unstable region bounded by the binodal line. There should exist a region in the phase diagram where the blend is a single-phase system (in which only microphase transition is operative). This region is proposed to locate at  $f_b > 0.86$ . When the temperature is raised, the microphases in the respective macrodomains underwent order–disorder transition; however, under the maximum accessible temperature (ca. 200 °C) the blends were still biphasic although the respective macrophases were disordered with only thermal concentration fluctuations.

The present study has reached the conclusions that it is essentially implausible to induce the transformation of microdomain morphology for rod–coil block copolymers through blending with the corresponding coil homopolymer even when the molecular weight of the copolymer is only 1/3 that of the coil block. Intuitively, this could be explained by the fact that the rod–rod attraction (i.e., the tendency of the rod to pack closely in lateral dimension) is so strong that a uniform solubilization of the homopolymer into the microdomains would cause the coil block to stretch excessively, which is entropically unfavorable (i.e., the loss of conformational entropy associated with such a stretching cannot be compensated by the gain of entropy of mixing). However, if such a wet-brush mixing is unfavorable, then why does not the diblock copolymer accommodate all the homopolymer chain into the coil microdomain by allowing them to form a dry-brush mixture with the coil blocks?

To explain the phase behavior observed in the present study, one has to be aware of the fact that it is not the local interaction between the PMMA blocks and h-PMMA that dictates the phase behavior of the blends. It is actually the interaction between the whole rod–coil diblock and h-PMMA that determines the miscibility. In this case, one has to treat the whole diblock molecule as one component and h-PMMA as the other component. The uniform mixing between h-PMMA and the whole diblock copolymer is unfavorable because the gain of entropy upon mixing with the rigid rods (which do not have conformational degree of freedom) is extremely small, and more importantly, there is a strong tendency for the rods to self-associate due to strong rod–rod attraction and the intrinsically strong repulsion (large  $\chi$  value) between DEH-PPV and PMMA. The unfavorable energy of mixing due to rod–rod attraction coupled with the very small gain in entropy of mixing prohibit the diblock copolymer to form miscible mixture with h-PMMA with even low molecular weight. During the solvent evaporation in the film casting, macrophase separation between the diblock and h-PMMA thus precedes the microphase separation, leading to a biphasic state. In the light of this argument, one will have to introduce another type of homopolymer that is able to form strong specific interaction with the coil block to compensate the rod–rod attraction to achieve a single-phase blend in which the homopolymer may

mix uniformly with the coil blocks in the microdomains to induce the morphological transformation.

## CONCLUSIONS

We have investigated the phase behavior of the blends of a rod-coil diblock copolymer, DEH-PPV-*b*-PMMA, with PMMA homopolymer, in which h-PMMA and PMMA block may form athermal mixture. The miscibility of the blends was studied as a function of  $f_b$  and  $\alpha$ , with the value of  $\alpha$  ranging from 0.31 to 1.23. The blends with  $f_b < \sim 0.86$  were found to undergo macrophase separation irrespective of the value of  $\alpha$ . The phase separation led to the formation of a copolymer-rich phase and a homopolymer-rich phase, in which microphase separation yielding a well-ordered lamellar structure and a sponge structure occurred, respectively. The h-PMMA chains interacted with PMMA blocks through dry brush. Therefore, microdomain morphology transformation induced by completely uniform solubilization of coil homopolymer into the selective microdomain was essentially inaccessible for the present blend system. The poor miscibility was attributed to the positive free energy of mixing between the whole rod-coil diblock and the corresponding homopolymer. The order-disorder transition revealed by the temperature-dependent SAXS experiments revealed that the two types of nanostructure disordered at different temperatures which lied closely to the melting point of DEH-PPV crystallites.

## AUTHOR INFORMATION

### Corresponding Author

\*E-mail: hlchen@che.nthu.edu.tw.

### Notes

The authors declare no competing financial interest.

## ACKNOWLEDGMENTS

This work was supported by the Ministry of Economic Affairs, Taiwan, under Grant 101-EC-17-A-09-S1-198, and the National Science Council, Taiwan, under Grant NSC 101-2623-E-007-013-IT.

## REFERENCES

- (1) Leibler, L. *Macromolecules* **1980**, *13*, 1602–1617.
- (2) Bates, F. S.; Fredrickson, G. H. *Annu. Rev. Phys. Chem.* **1990**, *41*, 525–557.
- (3) Bates, F. S.; Fredrickson, G. H. *Phys. Today* **1999**, *52*, 32–38.
- (4) Matsen, M. W. *Macromolecules* **1995**, *28*, 5765–5773.
- (5) Matsen, M. W. *Phys. Rev. Lett.* **1995**, *74*, 4225–4228.
- (6) Tanaka, H.; Hasegawa, H.; Hashimoto, T. *Macromolecules* **1991**, *24*, 240–251.
- (7) Koizumi, S.; Hasegawa, H.; Hashimoto, T. *Makromol. Chem., Macromol. Symp.* **1992**, *62*, 75–91.
- (8) Koizumi, S.; Hasegawa, H.; Hashimoto, T. *Macromolecules* **1994**, *27*, 6532–6540.
- (9) Olsen, B. D.; Segalman, R. A. *Macromolecules* **2005**, *38*, 10127–10137.
- (10) Olsen, B. D.; Segalman, R. A. *Macromolecules* **2006**, *39*, 7078–7083.
- (11) Olsen, B. D.; Segalman, R. A. *Macromolecules* **2007**, *40*, 6922–6929.
- (12) Sary, N.; Rubatat, L.; Brochon, C.; Hadziioannou, G.; Ruokolainen, J.; Mezzenga, R. *Macromolecules* **2007**, *40*, 6990–6997.
- (13) Ho, C. C.; Lee, Y. H.; Dai, C. A.; Segalman, R. A.; Su, W. F. *Macromolecules* **2009**, *42*, 4208–4219.
- (14) Singh, C.; Goulian, M.; Liu, A. J.; Fredrickson, G. H. *Macromolecules* **1994**, *27*, 2974–2986.
- (15) Reenders, M.; ten Brinke, G. *Macromolecules* **2002**, *35*, 3266–3280.
- (16) Müller, M.; Schick, M. *Macromolecules* **1996**, *29*, 8900–8903.
- (17) Netz, P. R.; Schick, M. *Phys. Rev. Lett.* **1996**, *77*, 302–305.
- (18) Li, W.; Gersappe, D. *Macromolecules* **2001**, *34*, 6783–6789.
- (19) Pryamitsyn, V.; Ganesan, V. *J. Chem. Phys.* **2004**, *120*, 5824–5838.
- (20) Ji, S. H.; Zin, W. C.; Oh, N. K.; Lee, M. *Polymer* **1997**, *38*, 4377–4380.
- (21) Tao, Y. F.; Olsen, B. D.; Ganesan, V.; Segalman, R. A. *Macromolecules* **2007**, *40*, 3320–3327.
- (22) Sary, N.; Mezzenga, R.; Brochon, C.; Hadziioannou, G.; Ruokolainen, J. *Macromolecules* **2007**, *40*, 3277–3286.
- (23) Sary, N.; Richard, F.; Brochon, C.; Leclerc, N.; Leveque, P.; Audinot, J. N.; Berson, S.; Heiser, T.; Hadziioannou, C.; Mezzenga, R. *Adv. Mater.* **2010**, *22*, 763–768.
- (24) Förster, S.; Timmann, A.; Konrad, M.; Schellbach, C.; Meyer, A.; Funari, S. S.; Mulvaney, P.; Knott, R. *J. Phys. Chem. B* **2005**, *109*, 1347–1360.
- (25) Olsen, B. D.; Alcazar, D.; Krikorian, V.; Toney, M. F.; Thomas, E. L.; Segalman, R. A. *Macromolecules* **2008**, *41*, 58–66.
- (26) Olsen, B. D.; Gu, X.; Hexemer, A.; Gann, E.; Segalman, R. A. *Macromolecules* **2010**, *43*, 6531–6534.
- (27) Zheng, J. X.; Xiong, H.; Chen, W. Y.; Lee, K.; Van Horn, R. M.; Quirk, R. P.; Lotz, B.; Thomas, E. L.; Shi, A.-C.; Cheng, S. Z. D. *Macromolecules* **2006**, *39*, 641–650.
- (28) Fetters, L. J.; Lohse, D. J.; Richter, D.; Witten, T. A.; Zirkel, A. *Macromolecules* **1994**, *27*, 4639–4647.
- (29) Roux, D.; Coulon, C.; Cates, M. E. *J. Phys. Chem.* **1992**, *96*, 4174–4187.
- (30) Jinnai, H.; Hasegawa, H.; Nishikawa, Y.; Agur Sevink, G. J.; Braunfeld, M. B.; Agard, D. A.; Spontak, R. J. *Macromol. Rapid Commun.* **2006**, *27*, 1424–1429.